processes

MDPI

Article

The Prediction of Flow Stress in the Hot Compression of a Ni-Cr-Mo Steel Using Machine Learning Algorithms

Tao Pan [1], Chengmin Song [1], Zhiyu Gao [2,*], Tian Xia [3] and Tianqi Wang [1]

[1] Institute of Structural Steel Research, Central Iron and Steel Research Institute, Beijing 100081, China; pantao@cisri.com.cn (T.P.); songchengmin0709@163.com (C.S.); wtq0719@163.com (T.W.)
[2] School of Materials Science and Engineering, Shenyang Ligong University, Shenyang 110159, China
[3] College of Materials Science & Engineering, Liaoning Technical University, Fuxin 123000, China; tianxia9708@163.com
* Correspondence: gaozhiyu@sylu.edu.cn

Abstract: The constitutive model refers to the mapping relationship between the stress and deformation conditions (such as strain, strain rate, and temperature) after being loaded. In this work, the hot deformation behavior of a Ni-Cr-Mo steel was investigated by conducting isothermal compression tests using a Gleeble-3800 thermal simulator with deformation temperatures ranging from 800 °C to 1200 °C, strain rates ranging from 0.01 s^{-1} to 10 s^{-1}, and deformations of 55%. To analyze the constitutive relation of the Ni-Cr-Mo steel at high temperatures, five machine learning algorithms were employed to predict the flow stress, namely, back-propagation artificial neural network (BP-ANN), Random Committee, Bagging, *k*-nearest neighbor (*k*-NN), and a library for support vector machines (libSVM). A comparative study between the experimental and the predicted results was performed. The results show that correlation coefficient (*R*), root mean square error (*RMSE*), mean absolute value error (*MAE*), mean square error (*MSE*), and average absolute relative error (*AARE*) obtained from the Random Committee on the testing set are 0.98897, 8.00808 MPa, 5.54244 MPa, 64.12927 MPa^2 and 5.67135%, respectively, whereas the metrics obtained via other algorithms are all inferior to the Random Committee. It suggests that the Random Committee can predict the flow stress of the steel more effectively.

Keywords: Ni-Cr-Mo steel; hot deformation; flow stress; constitutive model; machine learning algorithm; error evaluation

Citation: Pan, T.; Song, C.; Gao, Z.; Xia, T.; Wang, T. The Prediction of Flow Stress in the Hot Compression of a Ni-Cr-Mo Steel Using Machine Learning Algorithms. *Processes* **2024**, *12*, 441. https://doi.org/10.3390/pr12030441

Academic Editor: Blaž Likozar

Received: 5 February 2024
Revised: 18 February 2024
Accepted: 19 February 2024
Published: 22 February 2024

1. Introduction

High-strength low-alloy (HSLA) steels are widely used in various engineering structures, such as construction, automotive, shipbuilding, marine engineering, defense, etc., because they have excellent mechanical properties, including high strength, good plasticity and toughness, weldability, and low cost [1–3]. With the improvement of social demand and the development of modern industry, some new types of HSLA steels have been developed by means of reasonable chemical composition design, advanced material preparation, and modification processes [4,5]. Some computational materials science methods and tools have played a crucial role in composition design and process optimization and have been widely used in the research and development process of materials [6–8]. After the proposal of ICME and MGI [9,10], high-throughput material calculations, high-throughput experiments, and big data technology have received widespread attention, which has promoted the development of materials science and engineering [11], including research on material hot deformation behavior based on machine learning technology [12,13].

In industrial production and manufacturing, hot deformation technology is widely used in alloys to control microstructure and improve properties [14,15]. The microstructure evolution of materials during hot deformation is influenced by the combined effects of deformation conditions such as temperature, deformation rate, and deformation amount,

resulting in differences in the final performance of the materials. Manufacturing of fine grain steels is a good example of using hot deformation to control the microstructure and properties [16]. Accordingly, numerous studies have been carried out to study the hot deformation behavior of various materials and the creation of constitutive models, such as traditional ordinary carbon steel [17], aluminum alloy [15], magnesium alloy [18], titanium alloy [19], superalloy [14], as well as advanced materials such as high/medium entropy alloys [20,21], amorphous alloy [22], and so on. Zhao et al. [23] conducted isothermal compression tests for a low-carbon (0.05C) and a medium-carbon (0.38C) vanadium microalloyed steel at temperatures ranging from 900 to 1050 °C and strain rates ranging from 0.01 to 30 s^{-1}. Liu et al. [15] developed a physical-based diffusion constitutive model for Al-Mg-Si alloy, and the model described the flow behavior of the alloy accurately. Jalali et al. [24] studied compressive deformation behavior for $Zr_{33}Hf_8Ti_6Cu_{32}Ni_{10}Co_5Al_6$ high-entropy bulk metallic glass (HEBMG) and $Cu_{47}Zr_{47}Al_6$ low-entropy bulk metallic glass (BMG) at room temperature and high temperatures of 710 K and 730 K and found that the HEBMG alloy and BMG alloy have similar hot deformation behavior, but the HEBMG alloy withstood more stresses than the BMG alloy under similar testing conditions. However, few studies have reported the hot deformation behavior and constitutive analysis of Ni-Cr-Mo steel. Some existing studies have focused on the microstructure and properties regulation and fine characterization of steel plate thickness section after quenching and tempering [25–27].

Scholars classify the modeling of flow curves during hot deformation into three types: phenomenological model, physical model, and artificial neural network (ANN) algorithm [19,28]. The Arrihenius-type model proposed by Sellars et al. [29] is a typical phenomenological constitutive model, which is widely used for material constitutive analysis, and some scholars have proposed improved models [30]. The physics-based models are more complex, while the conventional ANN models require a lot of experimental data. Some studies have combined physical laws with ANN algorithms and achieved good results [31]. However, it should also be noted that, on the one hand, the construction of phenomenological and physical models is particularly sensitive to data and is usually based on some assumptions; on the other hand, conventional ANN models converge slowly and may fall into local optimal solutions [19]. All these shortcomings limit the application of the above methods, which is the reason why scholars keep exploring new constitutive analysis methods.

As is well known, in recent years, machine learning technology has developed rapidly and has been widely applied in the field of materials research, including alloy design [32,33], microstructure recognition [34], performance prediction [35], and process optimization [36], as well as the applications mentioned earlier in material hot deformation behavior and constitutive modeling. Wang et al. [37] used a machine learning algorithm based on singular value decomposition and deep neural networks to build metamodels for constitutive models, which not only assists in parameter fitting but also facilitates the understanding and analysis of constitutive models. Wen et al. [38] proposed a machine learning-assisted physical model to predict the flow behavior and microstructure evolution of a novel FGH4113A superalloy during thermomechanical processing and compared the predicted values with experimental data to show that the prediction accuracy is better than the traditional model. There are a variety of machine learning algorithms, and different algorithms are suitable for different situations, depending on the type of problem to be solved and the quality of the data set. For the same problem, one algorithm may not give the best result. Therefore, we need to find the best algorithm and the optimal parameter settings from multiple algorithms. In this work, five different machine learning algorithms were selected for the constitutive analysis of a Ni-Cr-Mo steel during the hot deformation process, including back-propagation artificial neural network (BP-ANN), Random Committee, Bagging, *k*-nearest neighbor (*k*-NN), and a library for support vector machines (libSVM). The results obtained by the machine learning algorithms were evaluated statistically by

using the experimental data of the hot compression test, and the prediction capability and generalization of the model were verified.

2. Experimental Materials and Methods

2.1. Material

The nominal chemical composition of the studied Ni-Cr-Mo steel is listed in Table 1. The as-received steel was industrially prepared by casting, electroslag remelting, and hot rolling to obtain uniform fine-grained microstructure and mechanical properties.

Table 1. Nominal chemical composition of the studied Ni-Cr-Mo steel (wt.%).

Element	C	Si	Ni	Cr	Mo	V	Mn	Fe
Content	0.08	0.25	4.5	Cr + Mo + V > 1.0			0.6	Bal.

2.2. Uniaxial Hot Compression Tests

Cylindrical specimens with a diameter of 8 mm and a height of 15 mm were cut from the rolled steel along the rolling direction using the wire electrical discharge machining technique, and their surfaces were polished to a bright finish using grinding machine. Single-pass uniaxial hot compression tests were conducted on a Gleeble-3800 thermo-simulator with resistance heating to characterize the flow characteristics of the Ni-Cr-Mo steel, and the temperature of the specimens was detected using thermocouples that were welded onto the side of the specimens. The specimens were first heated to 1200 °C at a rate of 10 °C/s and held for 300 s to obtain single-phase austenite, then cooled to different deformation temperatures (900 °C, 1000 °C, 1100 °C, 1200 °C) at a rate of 5 °C/s and held for 10 s, and then compressed to the nominal strain of 55% with a constant strain rate (ranging from 0.01 to 10 s^{-1} with interval of an order of magnitude). To reduce the friction between the specimens and the equipment and avoid adverse effects on the test results, thin graphite sheets and lubricants were placed between the specimens and the indenter. All the deformed specimens were preserved by room temperature water quenching immediately for microstructure observation. Figure 1 shows the schematic illustration of the hot compression tests.

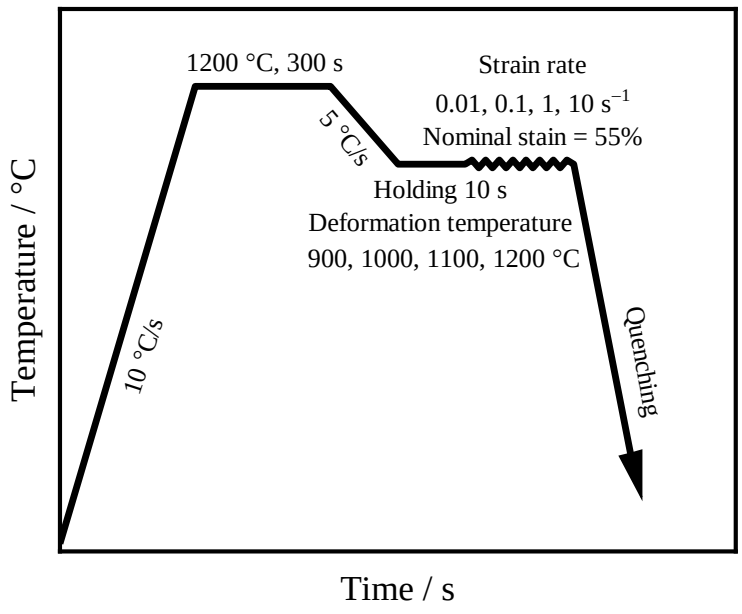

Figure 1. Schematic diagram of the uniaxial hot compression experiments.

2.3. Establishment of Machine Learning Models

2.3.1. Data Pre-Processing

The results of hot compression tests will provide input data for constitutive analysis in the subsequent section. In general, there are many quality issues in the raw dataset, such as data redundancy and data fluctuations [39]; therefore, pre-processing is necessary before training models. Data cleaning, normalization, and feature screening are commonly used data pre-processing methods and can improve the data quality, which is the premise of obtaining high-precision prediction [40].

Firstly, data cleaning methods were carried out to eliminate the effects of abnormal data, such as rheological data that was excessively large or small. Then, we used Origin to perform data smoothing to dispose of the fluctuations and irregularities in the experimental flow curves, which is performed by fitting a high-order polynomial method. Finally, in order to facilitate machine learning training and testing with rheological data obtained by the hot compression tests and to uniformly evaluate the accuracy of flow stress predicted by machine learning algorithms, interpolation processing was carried out based on the given true strain values (ranging from 0.05 to 0.8 with an interval of 0.05).

Figure 2 shows the comparison of the original data, smoothed data, and interpolated data under the condition of deformation temperature of 1000 °C and deformation rate of 0.01 s^{-1} and 10 s^{-1}, respectively. Obviously, the pre-processed data can well reflect the deformation trend of the original rheological data, exclude data interference, and be used to predict the flow stress of the Ni-Cr-Mo steel.

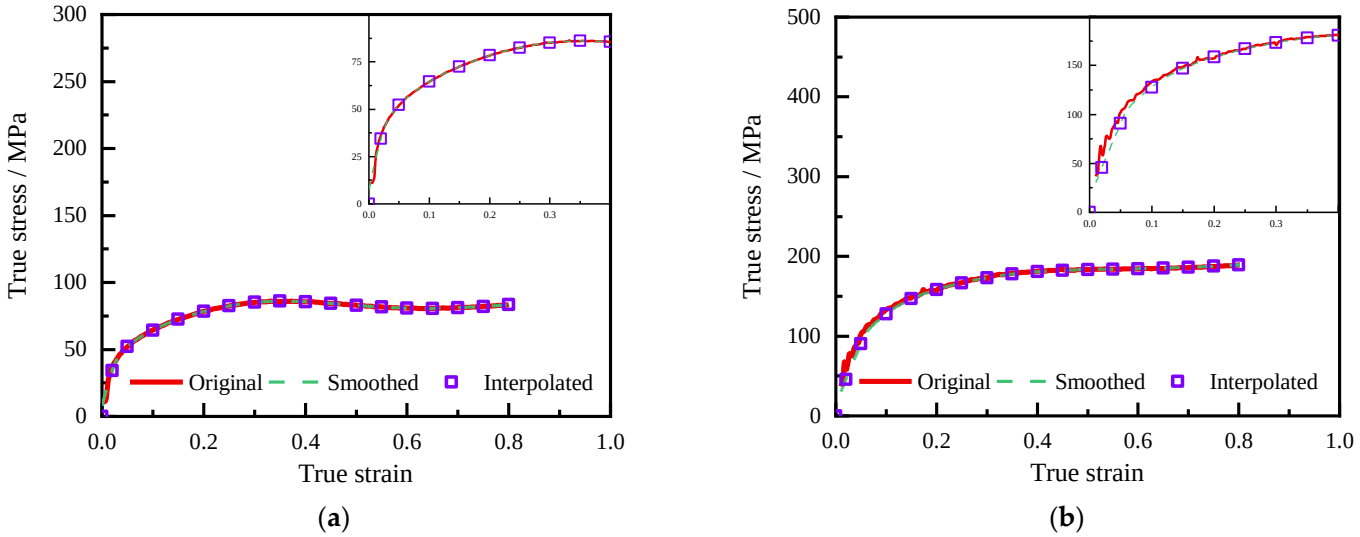

Figure 2. Comparison between the pre-processing results of experimental rheological data and the original data under temperature of 1000 °C with a strain rate of (**a**) 0.01 s^{-1} and (**b**) 10 s^{-1}.

Three main factors affecting the flow stress are deformation temperature, strain rate, and strain, which were selected as input features for the machine learning models, and stress was used as output parameter. The minimum, maximum, mean, and standard deviation of the input features are listed in Table 2. Obviously, the deformation parameters during hot compression have different physical meanings and vary greatly in numerical values. In order to improve the convergence reliability and speed of machine learning model during training and ensure that the input features have the same numerical weight, the input features must be normalized [41,42]. Therefore, linear Equation (1) was used to convert all the input data into the range of 0–1, which was carried out to obtain a dimensionless numerical representation of the input features and eliminate the difference in the numerical weights.

$$x_{\text{norm}} = \frac{x - x_{\text{min}}}{x_{\text{max}} - x_{\text{min}}} \quad (1)$$

where x denotes the original input data, x_{norm} denotes the normalized data corresponding to x, and x_{min} and x_{max} are the minimum or maximum values corresponding to x within the original input data, respectively.

Table 2. Minimum, maximum, mean, and standard deviation of input features.

Features	Minimum	Maximum	Mean	Standard Deviation
Temperature (°C)	800	1200	1023.333	128.045
Strain rate (s^{-1})	0.01	10	2.343	3.884
Strain	0.05	0.8	0.397	0.239

To train and test the machine learning model, the 304 data points obtained through pre-processing were randomly divided into a training set and a testing set, with the training set consisting of 244 data points and the testing set consisting of 60 data points. During the training of the model, we can use k-fold cross-validation technique to split the training set into training part and validation part.

2.3.2. Modeling

Due to the output parameter being numerical, a regression model with high predictive capability should established. In terms of evaluation metrics, predicted results of the model should exhibit a high correlation coefficient and low root mean square error, among other metrics that will be introduced later. Machine learning algorithms such as back-propagation artificial neural network (BP-ANN), Random Committee, Bagging, *k*-NN, and libSVM were chosen to predict flow stress in this paper. The above-mentioned machine learning algorithms were implemented by Weka 3.9.6 [43,44]. Random Tree derived from the decision tree algorithm was selected as the base learner for Random Committee and Bagging in this paper, with the seed of 2, the decimal places of 5, and the *K* value being the default value of Weka. The hyperparameter settings were a reasonable selection, tuning, and combination based on considering the prediction accuracy and generalization of the above machine learning models. To enhance the predictive ability of machine learning algorithms, a 10-fold cross-validation method was used to evaluate the models [45]. Flow chart of the model training and evaluation process is shown in Figure 3, and the characteristics and specific implementation settings of each algorithm are introduced as follows.

BP-ANN is an error back-propagation computational model that mimics the structure and function of biological neural networks. It can build a complex model efficiently by training data, which reflects the nonlinear relationship between input and output variables [46,47]. In this study, the deformation temperature, strain rate, and strain were taken as input layers, and flow stress was taken as output layer. The BP-ANN consisted of three hidden layers, with 4, 10, and 4 nodes, respectively. The learning rate of the network was 0.1, and the momentum coefficient was 0.1.

Random Committee is a type of ensemble learning algorithm that combines predictions from multiple classifiers trained on different random subsets of the training data to improve classification performance. A Random Committee model was developed for predicting flow stress in this work, with a seed number of 6, an iteration number of 15, a decimal place of 5, and an execution slot number of 5.

Bagging, also known as bootstrap aggregating, is an ensemble learning method in machine learning as well. It trains multiple base learners in parallel through random sampling with placement and then combines these base learners to form a strong learner to improve the accuracy and stability of prediction results and prevent overfitting. As mentioned above, Random Tree is selected as the base learner for the Bagging algorithm in

this article. Meanwhile, the number of batch sizes in this algorithm is preferably 100, and the number of decimal places is set to 5.

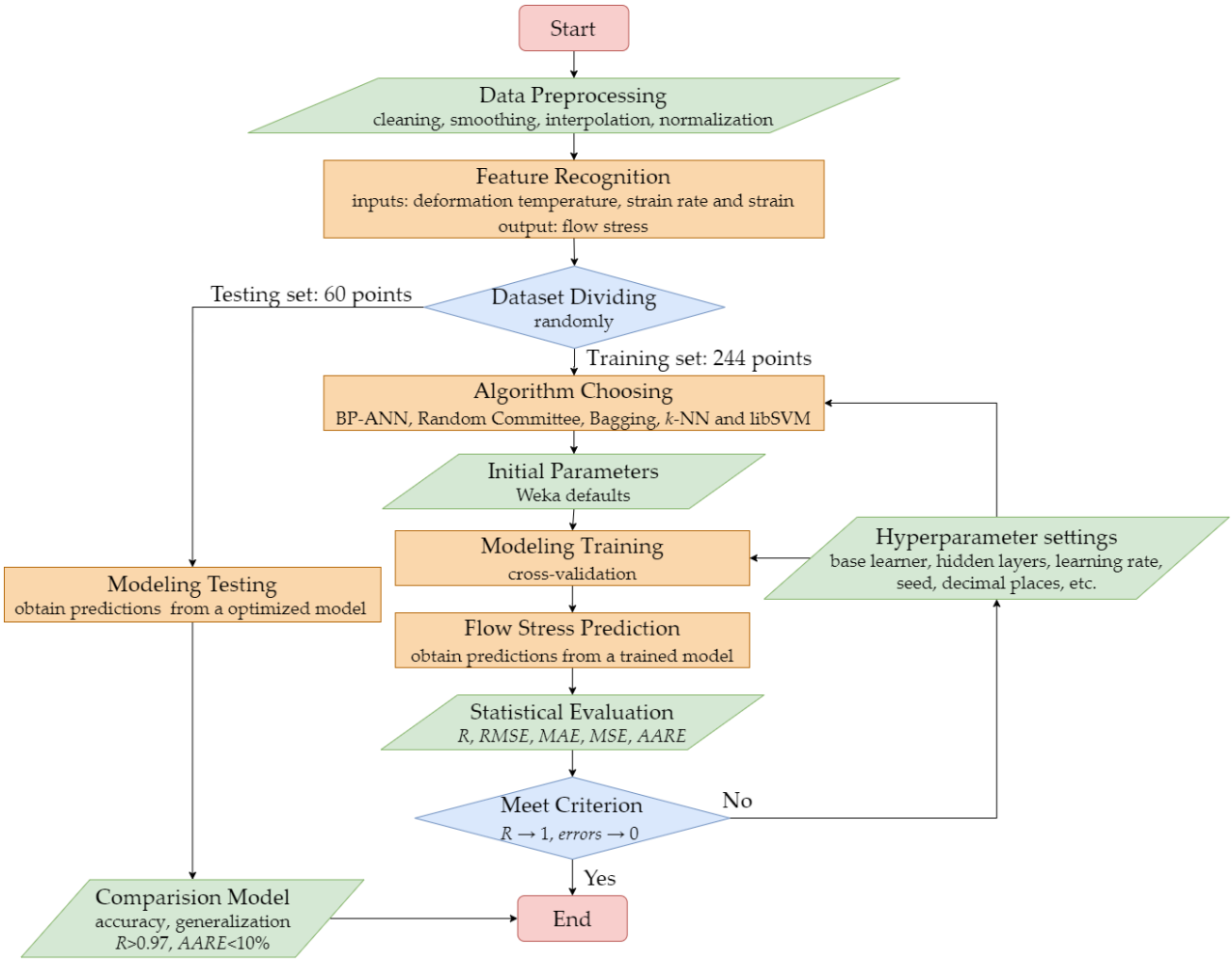

Figure 3. Flow chart showing the training process and turning parameters of the algorithms.

k-NN, a lazy learning algorithm, is recognized for its stability and simplicity, and the hyperparameter *k* of this work was set to 3 after comparison, with a decimal place of 5, and the default values of Weka are maintained for other options.

LibSVM is an integrated software package (library) for support vector machines (SVM), which is capable of solving classification and regression problems. It has high running efficiency compared to the sequential minimal optimization (SMO) algorithm [48]. Additionally, it supports multiple kernel functions and various SVM formulas. The nu-SVR (regression) was selected as the SVM model for this article, with a cost parameter set preferably to 100,000.0, while others remained at the default values of Weka.

2.3.3. Model Comparison and Evaluation

The hot deformation constitutive models of the Ni-Cr-Mo steel at elevated temperatures were established using the machine learning algorithms mentioned above. The experimental and predicted values of flow stress for the steel under various deformation parameters were then compared. Correlation coefficient (*R*), root mean square error (*RMSE*), mean absolute value error (*MAE*), mean square error (*MSE*), and average absolute

relative error (*AARE*) were utilized to evaluate the accuracy of the models and validate their predictability, illustrated by Equations (2)–(6).

$$R = \frac{\sum_{i=1}^{n}\left(P_i - \overline{P}\right)\left(E_i - \overline{E}\right)}{\sqrt{\sum_{i=1}^{n}\left(P_i - \overline{P}\right)^2 \cdot \sum_{i=1}^{n}\left(E_i - \overline{E}\right)^2}} \quad (2)$$

$$RMSE = \sqrt{\frac{1}{n}\sum_{i=1}^{n}(P_i - E_i)^2} \quad (3)$$

$$MAE = \frac{1}{n}\sum_{i=1}^{n}|P_i - E_i| \quad (4)$$

$$MSE = \frac{1}{n}\sum_{i=1}^{n}(P_i - E_i)^2 \quad (5)$$

$$AARE = \frac{1}{n}\sum_{i=1}^{n}\left|\frac{P_i - E_i}{E_i}\right| \times 100\% \quad (6)$$

where E_i and P_i are the experimental value and predicted value of flow stress, respectively, $\overline{E}$ and $\overline{P}$ are the mean values of the experimental (E_i) and predicted (P_i) data, respectively, and n is the total number of data.

3. Results and Discussion

3.1. True Stress–Strain Curve Analysis

The relationship between the flow stress and strain of the Ni-Cr-Mo steel at different compression deformation temperatures and strain rates is shown in Figure 4. The compression test was conducted with a deformation amount of 55%, which means the corresponding total true strain is 0.8. In order to visually compare the stress levels under different deformation conditions, the maximum value of the vertical coordinate in each true stress–strain curve is set to the same value. It can be observed that the variation of the flow stress is affected significantly by the deformation rate and deformation temperature. Comparing the flow stress at the same deformation temperature, it is evident that the stress increases significantly with the increase in deformation rate, and it decreases significantly with the increase in deformation temperature at the same deformation rate. Similar conclusions about flow behavior were also reported in other materials by Kong [14] et al. and Wu [49] et al. The competition mechanism between work hardening and dynamic softening during compression deformation determines the trend of the flow curve [47], and from a microscopic perspective, it is caused by the generation and entanglement of a large number of dislocations, as well as the competitive formation of new grains under appropriate strain and temperature conditions. As shown in Figure 4, on the one hand, the trend of flow stress shows four typical stages, namely, the work hardening stage, transition stage, softening stage, and steady-state stage, when deformation occurs at a low strain rate and a high temperature, for example, the curves at a strain rate of 0.01 s^{-1} and temperatures of 1000 °C and 1100 °C or at a strain rate of 0.1 s^{-1} and temperatures of 1100 °C and 1200 °C. On the other hand, the curves at high strain rates and low temperatures exhibit a continuous hardening characteristic, which is because, under such deformation conditions, it is not conducive to the occurrence of softening phenomena such as dynamic recovery (DRV) and dynamic recrystallization, as shown in Figure 4a,b.

3.2. Analysis of Training Set Results

In this study, the hot compression deformation constitutive models of the Ni-Cr-Mo steel at high temperatures were constructed using the BP-ANN, the Random Committee, the Bagging, the *k*-NN, and the libSVM, respectively. The predicted and experimental values of flow stress for the experimental steel under various deformation conditions were then compared.

The comparative graphs of the five algorithms at various deformation conditions are shown in Figure 5. According to Figure 5, it is evident that the Random Committee algorithm exhibits a significant advantage in the predictive capability of flow stress compared to the other algorithms. The trends of dynamic hardening, softening, and steady on the flow curves can be well described by the Random Committee algorithm. The predicted flow stress using libSVM and BP-ANN methods deviates significantly from the experimental values, especially for curves with strain rates of 0.01 s^{-1} and 0.1 s^{-1}. This indicates that these two algorithms have poor predictive capability in the current dataset and algorithm parameter settings.

Fitting points were plotted with experimental flow stress on the horizontal axis and predicted flow stress on the vertical axis to reflect the performance of the training set [19,40]. The closer the data points are to the $y = x$, the higher the prediction ability of the model is. As shown in Figure 6, the data points obtained by the Random Committee algorithm mostly fall on the $y = x$, indicating that this method has the best predictive ability, followed by the Bagging algorithm with the second-best prediction performance, while the libSVM, *k*-NN, and BP-ANN algorithms display relatively poor prediction performance.

The performance of the algorithms for the training set is further described quantitatively by the evaluation metrics mentioned earlier, including *R*, *RMSE*, *MAE*, *MSE*, and *AARE*. All these metrics can be calculated using Equations (2)–(6) and are listed in Table 3. As can be seen from the table, the metrics of the predicted and experimental flow stress values for the Random Committee are 0.99987, 1.02064 MPa, 0.69132 MPa, 1.04172 $MPa^{2,}$ and 0.67847%, respectively. Compared with the Bagging algorithm, libSVM algorithm, *k*-NN algorithm, and BP-ANN algorithm, the *R* value of Random Committee shows an increase of 0.00164, 0.01333, 0.01387, and 0.01710, respectively, while the *RMSE* value shows a decrease of 2.75567, 9.40012, 9.45247, and 10.89415, respectively, and the *AARE* value shows a decrease of 0.01548, 0.06051, 0.06219, and 0.08401, respectively. In addition, the *MAE* decreased by 1.73985, 6.82063, 6.46506, and 8.65923, respectively, and the *MSE* decreased by 13.21884, 107.55072, 108.64450, and 140.92054, respectively.

The *R* is a commonly used statistical parameter that characterizes the linear correlation level between predicted and experimental values, and a value of *R* close to 1 indicates a better fitting [50]. *RMSE*, *MAE*, *MSE*, and *AARE* are metrics that measure the difference between the predicted and experimental values, and the smaller the value of the metric, the smaller the prediction error [50,51]. These evaluation results demonstrate that the Random Committee algorithm established in this study can effectively predict the high-temperature flow behavior of the Ni-Cr-Mo steel for the training set with the maximum *R* (closest to 1) and the minimum deviation metrics (closest to 0), while the Bagging algorithm has good evaluation indexes, and its predictive capability is slightly lower than that of the Random Committee.

Table 3. Evaluation metrics for the five machine learning algorithms: correlation coefficient (*R*), root mean square error (*RMSE*), mean absolute value error (*MAE*), mean square error (*MSE*), and average absolute relative error (*AARE*).

Metrics	*R*	*RMSE* (MPa)	*MAE* (MPa)	*MSE* (MPa^2)	*AARE*
Random Committee	0.99987	1.02064	0.69132	1.04172	0.67847%
k-NN	0.98600	10.47312	7.15638	109.68620	6.89704%
Bagging	0.99822	3.77632	2.43118	14.26056	2.22691%
libSVM	0.98654	10.42077	7.51196	108.59240	6.72997%
BP-ANN	0.98277	11.91479	9.35055	141.96230	9.07926%

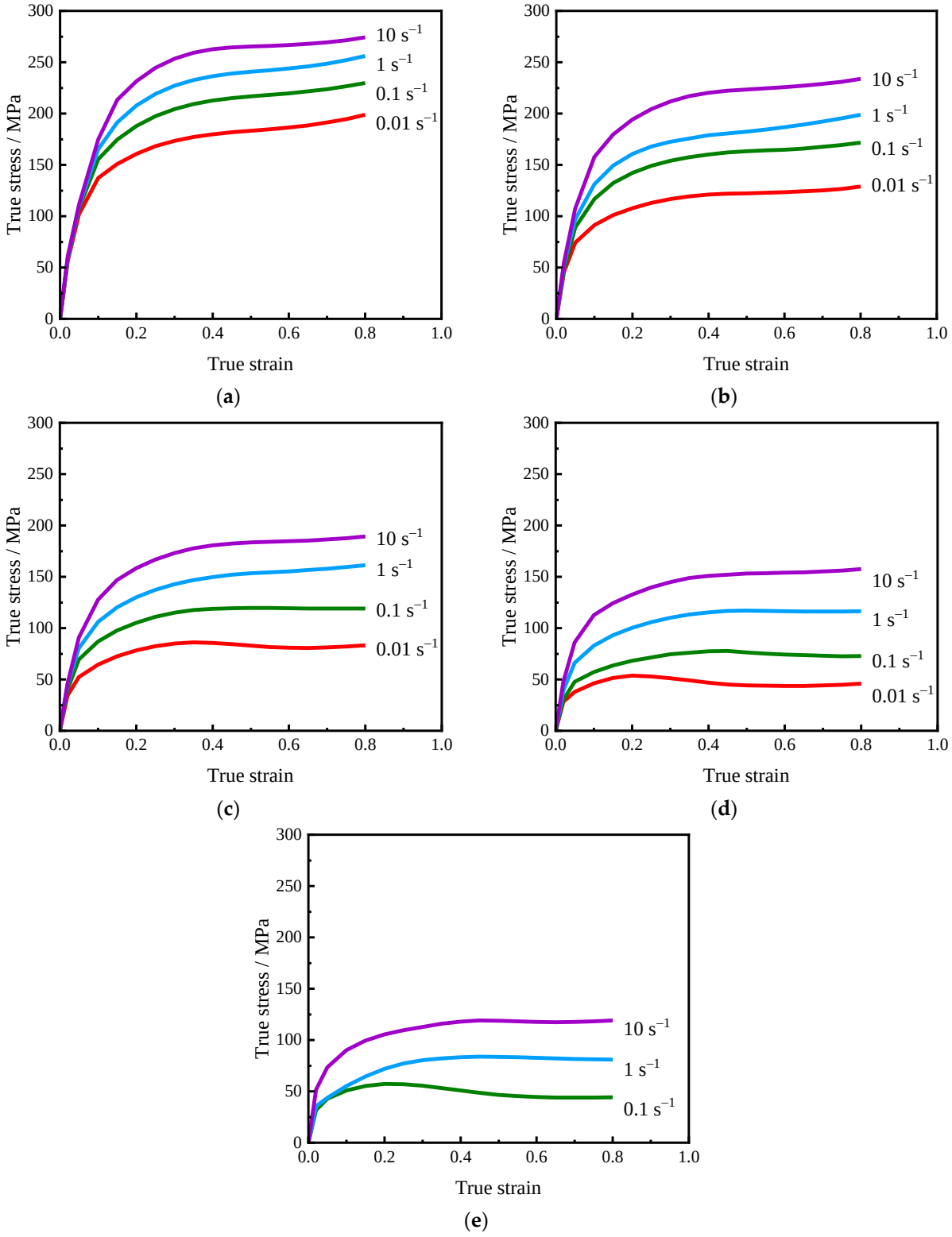

Figure 4. True stress–strain curves of the Ni-Cr-Mo steel compressed under various deformation conditions: (**a**) 800 °C; (**b**) 900 °C; (**c**) 1000 °C; (**d**) 1100 °C; (**e**) 1200 °C.

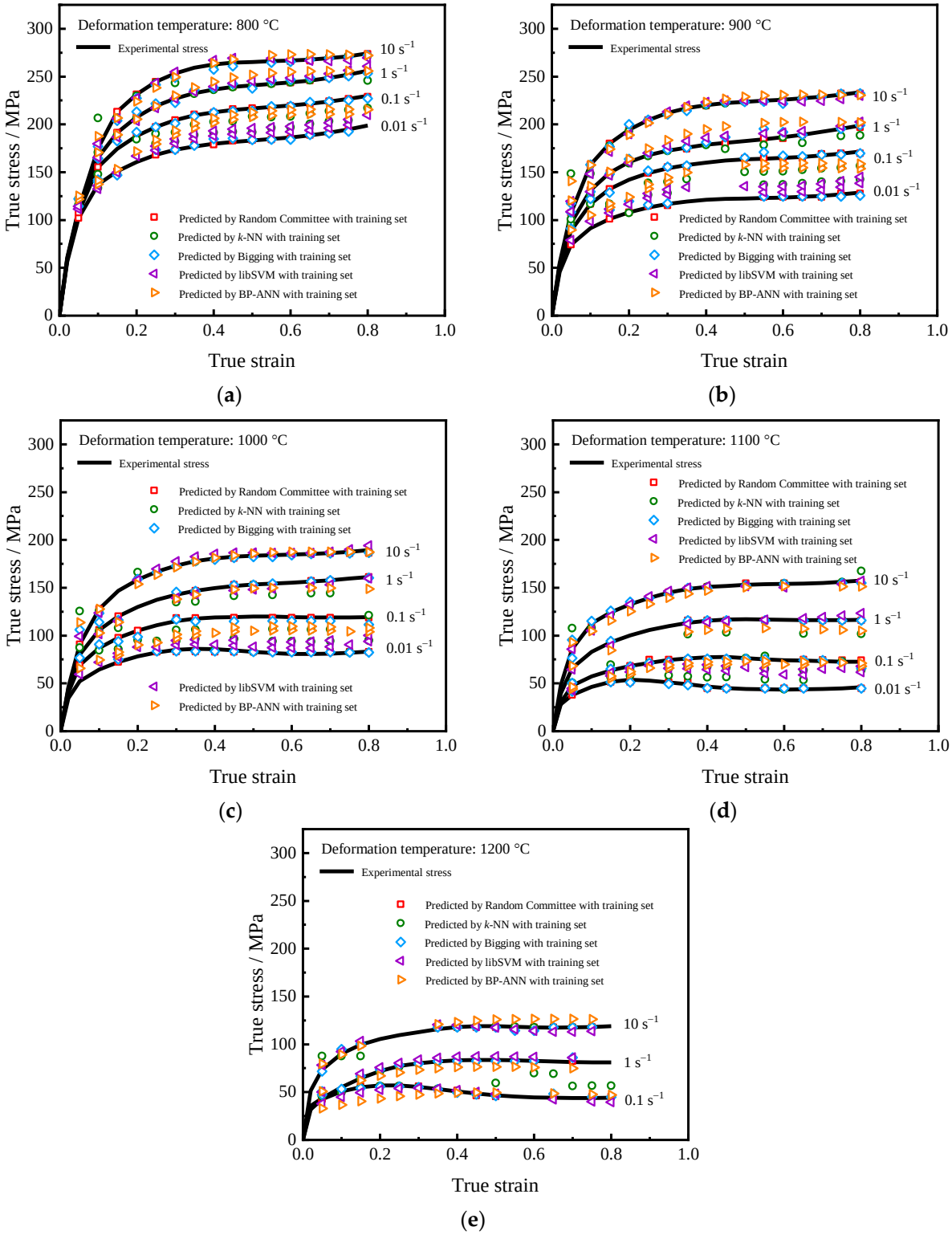

Figure 5. Comparison of experimental and predicted stress calculated by five algorithms on training set: (**a**) 800 °C; (**b**) 900 °C; (**c**) 1000 °C; (**d**) 1100 °C; (**e**) 1200 °C.

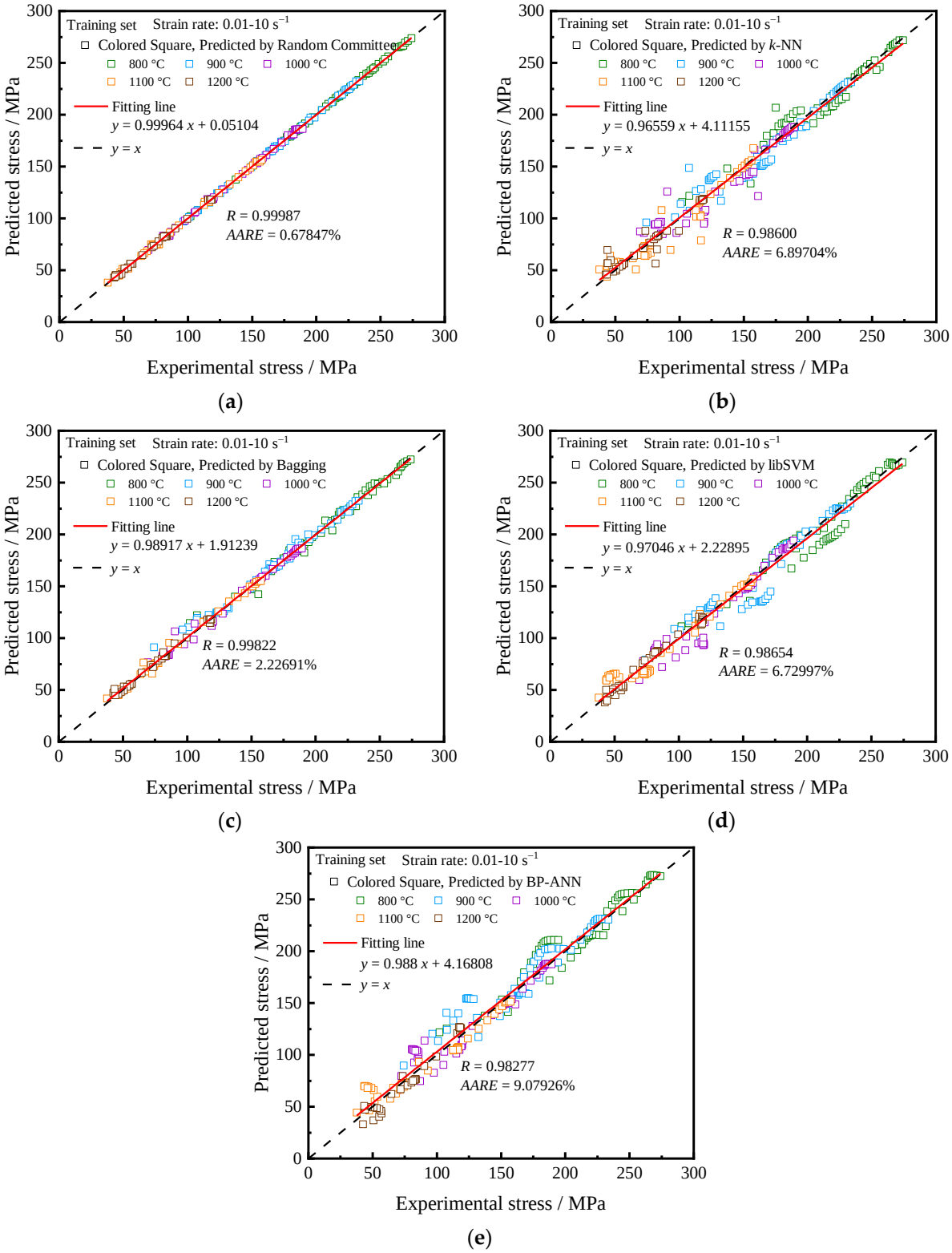

Figure 6. Correlation between experimental and predicted flow stress on training set with experimental temperatures of 800–1200 °C and strain rates of 0.01–10 s^{-1}: (**a**) Random Committee; (**b**) *k*-NN; (**c**) Bagging; (**d**) libSVM; (**e**) BP-ANN.

3.3. Analysis of Testing Set Results

The testing set was used to check the generalization capability of the models mentioned above. All the 60 items of data in the testing set were randomly selected and different from the training set data, ensuring that the prediction results were highly reliable.

Figure 7 compares the prediction accuracy of the constitutive relationship for the Ni-Cr-Mo steel during hot compression using the five machine learning algorithms on the testing set. It can be seen from the figure that the flow stress predicted by the Random Committee algorithm agrees well with the experimental data under different deformation conditions, with R being 0.98897 and $AARE$ being 5.67135%. Obviously, the Random Committee algorithm is the top choice for prediction, with the Bagging and libSVM algorithms coming in a close second. Meanwhile, for other algorithms, namely the k-NN and BP-ANN, the predicted values have a large deviation from the experimental values.

Figure 8 shows the quantitative evaluation results of correlation (R) and predictive error ($RMSE$, MAE, MSE, and $AARE$) of different machine learning algorithms used in this study. From the shape of the area enclosed by the adjacent evaluation metric connecting lines of each machine learning algorithm in the radar map, it can be seen that the sharper the angle of a certain algorithm on the R-axis (vertical direction) and the narrower the span in the horizontal direction, the better the predictive performance of this algorithm. As shown in the figure, the red area enclosed by the Random Committee method exhibits this feature. In terms of quantitative analysis of evaluation metrics, the R values of the Random Committee, Bagging, and libSVM algorithms used for predicting flow stress are all above 0.97 (0.98897, 0.97898, and 0.97088, respectively), and the $AARE$ values are all less than 10% (5.67135%, 6.68647%, and 8.74252%, respectively), which indicates that these algorithms have a good prediction and generalization capabilities.

3.4. Comprehensive Analysis between Training and Testing Sets

To sum up, as shown in Figures 6 and 7, by comparing the predicted flow stresses of each model with the experimental values on the training set, as well as the testing set, the results reveal that the Random Committee model generally exhibits superior prediction performance, with most of the points being clustered around the 45° oblique line. Based on the distance of each point deviating from the 45° oblique line, the ranking of different algorithms in terms of flow stress prediction performance from high to low on both the training and testing sets is Random Committee, Bagging, libSVM, BP-ANN, and k-NN.

Using the evaluation metrics described in Equations (2)–(6), the comprehensive quantitative analysis for the prediction accuracy and generalization ability of the five developed machine learning models was conducted. As illustrated in Figure 9, when compared to the predictability of the remaining models, higher R values (higher than 0.97) and smaller error values ($RMSE$, MAE, MSE, and $AARE$) are obtained in both the training and testing sets for the Random Committee, Bagging, and libSVM models. Figure 9 also indicates that the invisibility of the testing set to the training process results in the evaluation metrics for the prediction results of the testing set being slightly inferior to those of the training set, and this feature is consistent across the different algorithms. Specifically, compared with the evaluation metrics on the training set, the R values of the Random Committee, Bagging, and libSVM models on the testing set decreased by 0.01090, 0.01924, and 0.01565, respectively. Meanwhile, the $RMSE$, MAE, MSE, and $AARE$ values of these three models increased by 6.98743 MPa, 6.83368 MPa, and 1.41829 MPa; 4.85111 MPa, 4.11039 MPa, and 0.92623 MPa; 63.08755 MPa^2, 98.31150 MPa^2, and 31.57096 MPa^2; and 4.99288%, 4.45956%, and 2.01255%, respectively. On the other hand, both BP-ANN and k-NN models obtain relatively high R values, with R values of 0.98277 and 0.98600 on the training set and 0.95629 and 0.90055 on the testing set, showing great linear correlation. However, the error values of these two models are relatively large, especially in the testing set, with $AARE$ values of 11.77017% and 17.81745, respectively. This indicates that the predictive capability of BP-ANN and k-NN models is inferior to other models in this paper. Moreover, it should be noted that the libSVM model has the smallest difference in evaluation metrics corresponding to the

training set and testing set, which indicates that it has the best generalization and excellent accuracy. Eventually, Random Committee, Bagging, and libSVM models obtain higher R values and smaller error values, fully demonstrating their superiority.

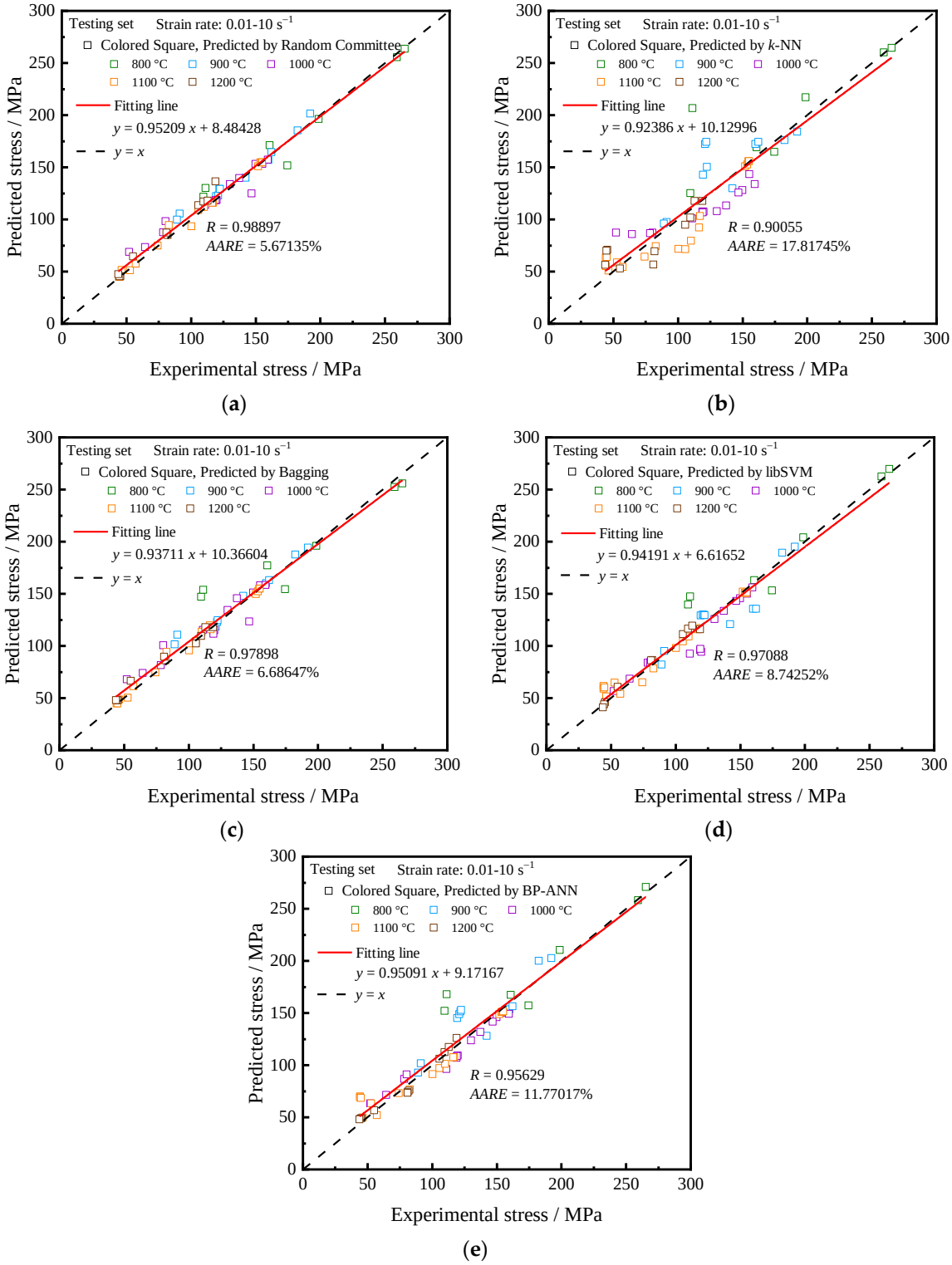

Figure 7. Correlation between experimental and predicted flow stress on testing set with experimental temperatures of 800–1200 °C and strain rates of 0.01–10 s^{-1}: (**a**) Random Committee; (**b**) *k*-NN; (**c**) Bagging; (**d**) libSVM; (**e**) BP-ANN.

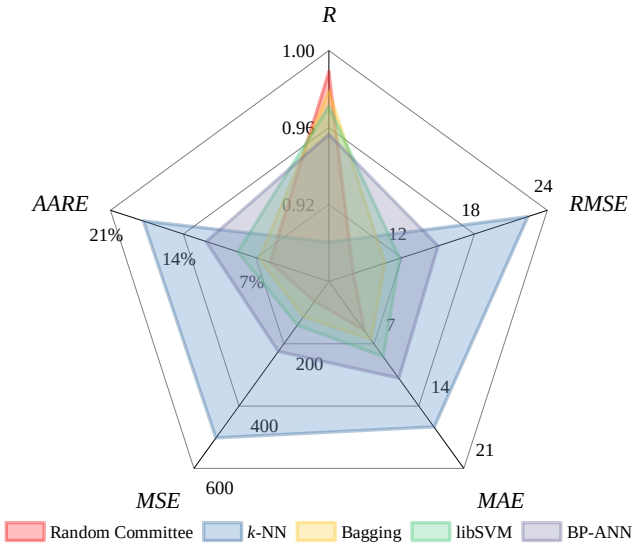

Figure 8. Comparison of flow stress prediction capabilities of different machine learning algorithms on the testing set, with experimental temperatures ranging from 800 to 1200 °C and strain rates ranging from 0.01 to 10 s^{-1}.

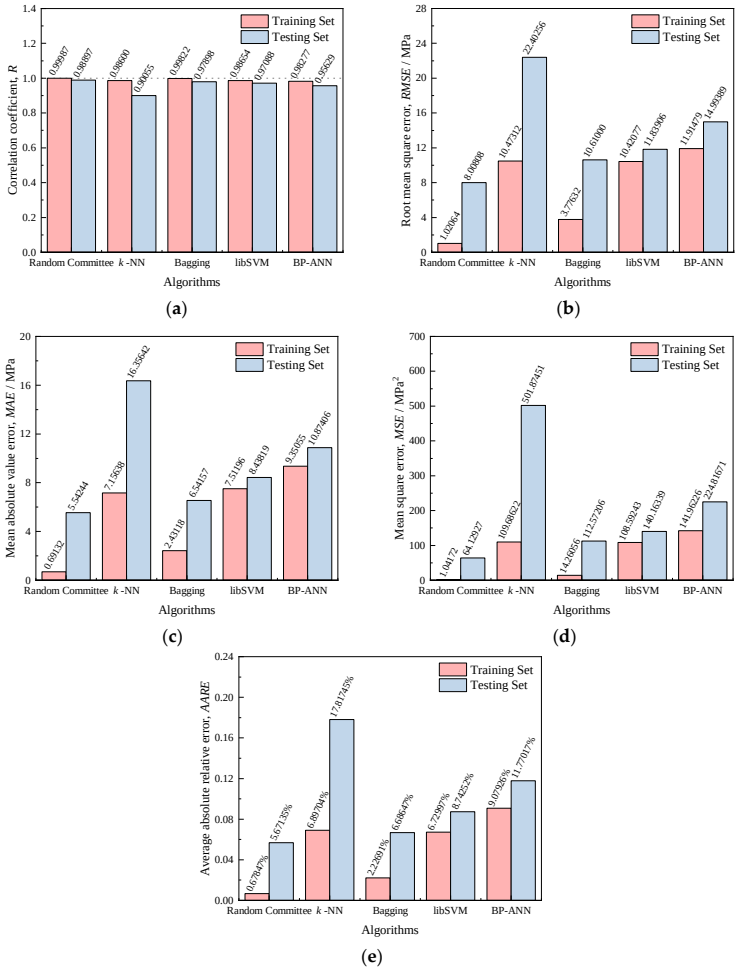

Figure 9. Evaluation metric values for five machine learning algorithms on the training and testing sets under all compression experimental parameters: (**a**) correlation coefficient, *R*; (**b**) root mean square error, *RMSE*; (**c**) mean absolute value error, *MAE*; (**d**) mean square error, *MSE*; (**e**) average absolute relative error, *AARE*.

4. Conclusions

Flow stresses of the Ni-Cr-Mo steel were predicted for various deformation parameters (temperature range of 800–1200 °C, strain rate of 0.01–10 s^{-1}) using different machine learning algorithms, including BP-ANN, Random Committee, Bagging, *k*-NN, and libSVM. All the data used in this study were obtained from hot compression experiments. All models were trained using descriptors, including the strain, temperature, and strain rate. The evaluation of the predicted flow stress results was based on statistical metrics, such as *R*, *RMSE*, *MAE*, *MSE*, and *AARE*. The *R*, *RMSE*, *MAE*, *MSE*, and *AARE* for the five models on the testing set are 0.95629, 14.99389 MPa, 10.87406 MPa, 224.81671 MPa^2, and 11.77017%; 0.98897, 8.00808 MPa, 5.54244 MPa, 64.12927 MPa^2, and 5.67135%; 0.97898, 10.61 MPa, 6.54157 MPa, 112.57206 MPa^2, and 6.68647%; 0.90055, 22.40256 MPa, 16.35642 MPa, 501.87451 MPa^2, and 17.81745%; and 0.97088, 11.83906 MPa, 8.43819 MPa, 140.16339 MPa^2, and 8.74252%, respectively. The Random Committee algorithm has excellent predictive capability due to its high correlation coefficient and low errors, followed by the Bagging and libSVM algorithms with higher prediction accuracy and generalization capability. The BP-ANN and *k*-NN exhibit the relatively high prediction errors, indicating poor generalization of these two algorithms. In addition, based on the fluctuation of each evaluation metric on the training set and the testing set, the libSVM algorithm has the best generalization.

Author Contributions: Conceptualization, methodology, and investigation, T.P. and Z.G.; software, T.X.; validation, T.P. and Z.G.; formal analysis, C.S.; resources, T.W.; data curation, C.S. and T.X.; writing—original draft preparation, T.P. and C.S.; writing—review and editing, Z.G.; visualization, T.X. and T.W. All authors have read and agreed to the published version of the manuscript.

Funding: This research has received no external funding.

Data Availability Statement: The data used in this study will be made available from the corresponding author upon reasonable request.

Conflicts of Interest: Authors Tao Pan, Chengmin Song and Tianqi Wang were employed by the company Central Iron and Steel Research Institute. The remaining authors declare that the research was conducted in the absence of any commercial or financial relationships that could be construed as a potential conflict of interest.

References

1. Dong, C.; Zhao, X. Dynamic recrystallization behavior and microstructure evolution of high-strength low-alloy steel during hot deformation. *J. Mater. Res. Technol* **2023**, *25*, 6087–6098. [CrossRef]
2. Hamada, A.; Khosravifard, A.; Ali, M.; Ghosh, S.; Jaskari, M.; Hietala, M.; Järvenpää, A.; Newishy, M. Micromechanical analysis and finite element modelling of laser-welded 5-mm-thick dissimilar joints between 316L stainless steel and low-alloyed ultra-high-strength steel. *Mater. Sci. Eng. A* **2023**, *882*, 145442. [CrossRef]
3. Cheng, H.; Luo, X.; Wu, X. Recent research progress on additive manufacturing of high-strength low-alloy steels: Focusing on the processing parameters, microstructures and properties. *Mater. Today Commun.* **2023**, *36*, 106616. [CrossRef]
4. Chen, X.; Huang, Y. Hot deformation behavior of HSLA steel Q690 and phase transformation during compression. *J. Alloys Compd.* **2015**, *619*, 564–571. [CrossRef]
5. Chen, C.; Chen, C.; Yang, J. Synergistic effect of austenitizing temperature and hot plastic deformation strain on the precipitation behavior in novel HSLA steel. *Mater. Sci. Eng. A* **2015**, *639*, 145–154. [CrossRef]
6. Costa E Silva, A. Challenges and opportunities in thermodynamic and kinetic modeling microalloyed HSLA steels using computational thermodynamics. *Calphad* **2020**, *68*, 101720. [CrossRef]
7. Dornelas, P.H.G.; Payão Filho, J.D.C.; Farias, F.W.C.; Moraes E Oliveira, V.H.P.; Moraes, D.D.O.; Zumpano Júnior, P. FEM-thermodynamic simulation methodology to predict the influence of t8/5 on the coarse grain heat-affected zone of a Cr-Mo low-alloy steel pipe. *J. Manuf. Process.* **2020**, *60*, 520–529. [CrossRef]
8. Pan, B.; Sun, H.; Xie, D.; Shang, S.; Li, N.; Carlson, B.E.; Li, Y.; Liu, Z.; Li, J. Influence of accelerated corrosion on Al/steel RSW joints by in situ compression tests. *Mater. Sci. Eng. A* **2024**, *889*, 145851. [CrossRef]
9. Ling, J.; Chen, W.; Sheng, Y.; Li, W.; Zhang, L.; Du, Y. A MGI-oriented investigation of the Young's modulus and its application to the development of a novel Ti–Nb–Zr–Cr bio-alloy. *Mater. Sci. Eng. C* **2020**, *106*, 110265. [CrossRef]
10. LI, D. Integrated Computational Materials Science: New paradigm for metal manufacturing. *Acta Metall. Sin.* **2018**, *54*, 129–130.
11. Xie, J.; Su, Y.; Zhang, D.; Feng, Q. A vision of Materials Genome Engineering in China. *Engineering* **2022**, *10*, 10–12. [CrossRef]

12. Li, H.; Wang, X.; Song, Y.; Li, Y.; Li, X.; Ji, Y. Physical metallurgy guided machine learning to predict hot deformation mechanism of stainless steel. *Mater. Today Commun.* **2023**, *36*, 106779. [CrossRef]
13. Li, D.; Liu, J.; Fan, Y.; Yang, X.; Huang, W. A preliminary discussion about the application of machine learning in the field of constitutive modeling focusing on alloys. *J. Alloys Compd.* **2024**, *976*, 173210. [CrossRef]
14. Kong, R.; Meng, B.; Ma, X.; Li, Y.; Zheng, L.; Zhu, Y.; Wan, M. Hot deformation behavior and microstructure evolution of Inconel 625 superalloy sheet. *J. Alloys Compd.* **2022**, *915*, 165367. [CrossRef]
15. Liu, S.; Pan, Q.; Li, M.; Wang, X.; He, X.; Li, X.; Peng, Z.; Lai, J. Microstructure evolution and physical-based diffusion constitutive analysis of Al-Mg-Si alloy during hot deformation. *Mater. Des.* **2019**, *184*, 108181. [CrossRef]
16. Langdon, T.G. Twenty-five years of ultrafine-grained materials: Achieving exceptional properties through grain refinement. *Acta Mater.* **2013**, *61*, 7035–7059. [CrossRef]
17. Saadatkia, S.; Mirzadeh, H.; Cabrera, J. Hot deformation behavior, dynamic recrystallization, and physically-based constitutive modeling of plain carbon steels. *Mater. Sci. Eng. A* **2015**, *636*, 196–202. [CrossRef]
18. Cao, F.; Sun, C.; Liu, S.; Liang, J.; Liu, R.; Guo, H.; Guo, N. Microstructures, hot tensile deformation behavior and constitutive modeling in a superlight Mg-2.76Li-3Al-2.6Zn-0.39Y alloy. *J. Alloys Compd.* **2022**, *896*, 163049. [CrossRef]
19. Liu, X.; Zhang, H.; Zhang, S.; Peng, W.; Zhou, G.; Wang, C.; Chen, L. Hot deformation behavior of near-β titanium alloy Ti-3Mo-6Cr-3Al-3Sn based on phenomenological constitutive model and machine learning algorithm. *J. Alloys Compd.* **2023**, *968*, 172052. [CrossRef]
20. Jiao, W.; Li, T.; Yin, G.; He, T.; Li, T.; Lu, Y. Hot deformation characteristics and microstructure evolution of Al20Co36Cr4Fe4Ni36 eutectic high entropy alloy. *Mater. Charact.* **2023**, *204*, 113180. [CrossRef]
21. Jiang, W.; Cao, Y.; Yuan, S.; Zhang, Y.; Zhao, Y. Creep properties and deformation mechanisms of a $Ni_2Co_1Fe_1V_{0.5}Mo_{0.2}$ medium-entropy alloy. *Acta Mater.* **2023**, *245*, 118590. [CrossRef]
22. Tao, P.; Zhang, W.; Chen, Y.; Si, J.; Zhu, K.; Huang, Z.; Yang, Y. Effect of high temperature deformation on the deformation behavior and thermodynamic properties of a Zr-based bulk amorphous alloy. *J. Alloys Compd.* **2022**, *907*, 164450. [CrossRef]
23. Zhao, H.; Qi, J.; Liu, G.; Su, R.; Sun, Z. A comparative study on hot deformation behaviours of low-carbon and medium-carbon vanadium microalloyed steels. *J. Mater. Res. Technol* **2020**, *9*, 11319–11331. [CrossRef]
24. Jalali, A.; Malekan, M.; Park, E.S.; Rashidi, R.; Bahmani, A.; Yoo, G.H. Deformation behavior of $Zr_{33}Hf_8Ti_6Cu_{32}Ni_{10}Co_5Al_6$ high-entropy bulk metallic glass and $Cu_{47}Zr_{47}Al_6$ low-entropy bulk metallic glass at room and high temperatures. *Mater. Sci. Eng. A* **2022**, *832*, 142499. [CrossRef]
25. Guo, K.; Pan, T.; Zhang, N.; Meng, L.; Luo, X.; Chai, F. Effect of microstructural evolution on the mechanical properties of Ni-Cr-Mo ultra-heavy steel plate. *Materials* **2023**, *16*, 1607. [CrossRef]
26. Guo, K.; Pan, T.; Meng, L.; Chai, F.; Luo, X. Morphology and crystallography of the coalescent structure in Ni-Cr-Mo industrial heavy steel plate. *Mater. Lett.* **2023**, *331*, 133446. [CrossRef]
27. Bansal, G.K.; Tripathy, S.; Chandan, A.K.; Rajinikanth, V.; Ghosh, C.; Srivastava, V.C.; Ghosh Chowdhury, S. Influence of quenching strategy on phase transformation and mechanical properties of low alloy steel. *Mater. Sci. Eng. A* **2021**, *826*, 141937. [CrossRef]
28. Feng, R.; Bao, Y.; Ding, Y.; Chen, M.; Ge, Y.; Xie, L. Three different mathematical models to predict the hot deformation behavior of TA32 titanium alloy. *J. Mater. Res.* **2022**, *37*, 1309–1322. [CrossRef]
29. Sellars, C.M.; McTegart, W.J. On the mechanism of hot deformation. *Acta Mater.* **1966**, *14*, 1136–1138. [CrossRef]
30. Xue, D.; Wei, W.; Shi, W.; Zhou, X.; Rong, L.; Wen, S.; Wu, X.; Qi, P.; Gao, K.; Huang, H.; et al. Microstructural evolution and constitutive analysis of Al-Mg-Zn-Er-Zr based on arrhenius-type and machine-learning algorithm. *Mater. Today Commun.* **2022**, *32*, 104076. [CrossRef]
31. Fuhg, J.N.; Bouklas, N. On physics-informed data-driven isotropic and anisotropic constitutive models through probabilistic machine learning and space-filling sampling. *Comput. Meth. Appl. Mech. Eng.* **2022**, *394*, 114915. [CrossRef]
32. Hu, M.; Tan, Q.; Knibbe, R.; Xu, M.; Jiang, B.; Wang, S.; Li, X.; Zhang, M. Recent applications of machine learning in alloy design: A review. *Mater. Sci. Eng. R* **2023**, *155*, 100746. [CrossRef]
33. Merchant, A.; Batzner, S.; Schoenholz, S.S.; Aykol, M.; Cheon, G.; Cubuk, E.D. Scaling deep learning for materials discovery. *Nature* **2023**, *624*, 80–85. [CrossRef]
34. Ma, X.; Yu, Y. Training tricks for steel microstructure segmentation with deep learning. *Processes* **2023**, *11*, 3298. [CrossRef]
35. Golmohammadi, M.; Aryanpour, M. Analysis and evaluation of machine learning applications in materials design and discovery. *Mater. Today Commun.* **2023**, *35*, 105494. [CrossRef]
36. Thakur, S.K.; Kumar Das, A.; Jha, B.K. Application of machine learning methods for the prediction of roll force and torque during plate rolling of micro-alloyed steel. *J. Alloy. Metall. Syst.* **2023**, *4*, 100044. [CrossRef]
37. Wang, J.; Zhu, B.; Hui, C.; Zehnder, A.T. Determination of material parameters in constitutive models using adaptive neural network machine learning. *J. Mech. Phys. Solids* **2023**, *177*, 105324. [CrossRef]
38. Wen, H.; Jin, J.; Tang, X.; Wang, X.; Yang, H.; Zhang, Y.; Zhang, M.; Deng, L.; Wei, Q.; Chen, J.; et al. Machine learning-assisted constitutive modeling of a novel powder metallurgy superalloy. *Int. J. Mech. Sci.* **2023**, *260*, 108654. [CrossRef]
39. Mirzadeh, H.; Najafizadeh, A.; Moazeny, M. Flow curve analysis of 17-4 PH stainless steel under hot compression test. *Metall. Mater. Trans. A* **2009**, *40*, 2950–2958. [CrossRef]

40. Huang, X.; Wang, H.; Xue, W.; Xiang, S.; Huang, H.; Meng, L.; Ma, G.; Ullah, A.; Zhang, G. Study on time-temperature-transformation diagrams of stainless steel using machine-learning approach. *Comput. Mater. Sci.* **2020**, *171*, 109282. [CrossRef]
41. Zhu, W.; Huo, W.; Wang, S.; Wang, X.; Ren, K.; Tan, S.; Fang, F.; Xie, Z.; Jiang, J. Phase formation prediction of high-entropy alloys: A deep learning study. *J. Mater. Res. Technol* **2022**, *18*, 800–809. [CrossRef]
42. Gao, Z.Y.; Zhao, F.; Gao, S.D.; Xia, T. Machine learning prediction of hardness in solid solution high entropy alloys. *Mater. Today Commun.* **2023**, *37*, 107102. [CrossRef]
43. Yuan, M.Y. *Data Mining and Machine Learning: WEKA Application Technology and Practice*, 2nd ed.; Tsinghua University Press: Beijing, China, 2016; pp. 35–81.
44. Witten, I.H.; Frank, E.; Hall, M.A.; Pal, C.J. *Data Mining: Practical Machine Learning Tools and Techniques*, 4th ed.; Morgan Kaufman: San Francisco, CA, USA, 2017; pp. 44–65.
45. Malakouti, S.M. Babysitting hyperparameter optimization and 10-fold-cross-validation to enhance the performance of ML methods in predicting wind speed and energy generation. *Intell. Syst. Appl.* **2023**, *19*, 200248. [CrossRef]
46. Chen, W.; Li, S.; Bhandari, K.S.; Aziz, S.; Chen, X.; Jung, D.W. Genetic optimized Al–Mg alloy constitutive modeling and activation energy analysis. *Int. J. Mech. Sci.* **2023**, *244*, 108077. [CrossRef]
47. Wei, Z.; Su, X.; Wang, D.; Feng, Z.; Gao, Q.; Xu, G.; Zu, G. Three-dimensional processing map based on BP-ANN and interface microstructure of Fe/Al laminated sheet. *Mater. Chem. Phys.* **2023**, *297*, 127431. [CrossRef]
48. Alam, M.T.; Ubaid, S.; Shakil; Sohail, S.S.; Nadeem, M.; Hussain, S.; Siddiqui, J. Comparative analysis of machine learning based filtering techniques using MovieLens dataset. *Procedia Comput. Sci.* **2021**, *194*, 210–217. [CrossRef]
49. Wu, C.; Han, S. Hot deformation behavior and dynamic recrystallization characteristics in a low-alloy high-strength Ni–Cr–Mo–V steel. *Acta Metall. Sin. (Engl. Lett.)* **2018**, *31*, 963–974. [CrossRef]
50. Gao, Z.Y.; Kang, Y.; Li, Y.S.; Meng, C.; Pan, T. Study on elevated-temperature flow behavior of Ni-Cr-Mo-B ultra-heavy-plate steel via experiment and modelling. *Mater. Res. Express* **2018**, *5*, 46520. [CrossRef]
51. Liu, C.; Wang, X.; Cai, W.; He, Y.; Su, H. Machine learning aided prediction of glass-forming ability of metallic glass. *Processes* **2023**, *11*, 2806. [CrossRef]